Influence of the processing route on the carbon nanotubes dispersion and creep resistance of 3YTZP/SWCNTs nanocomposites

Miguel Castillo-Rodríguez[1*], Antonio Muñoz[2], Ana Morales-Rodríguez[1,2], Rosalía Poyato[1], Ángela Gallardo-López[1,2] and Arturo Domínguez-Rodríguez[2**]

[1]Instituto de Ciencia de Materiales de Sevilla, CSIC-Universidad de Sevilla, Avda. Américo Vespucio 49, 41092 Sevilla, Spain

[2]Departamento de Física de la Materia Condensada, Facultad de Física, Universidad de Sevilla, Apartado 1065, 41080 (Sevilla), Spain

Abstract: 3YTZP matrix composites containing 2.5 vol.% of single-walled carbon nanotubes (SWCNT) were fabricated by Spark Plasma Sintering (SPS) at 1250 ºC, following different processing routines with the aim of optimizing the SWCNTs dispersion throughout the ceramic matrix. Microstructural characterization of the as-fabricated samples has been performed by means of scanning electron microscopy (SEM). The specimens have been crept at 1200 ºC to correlate creep resistance and SWCNTs distribution. There are no creep experimental results on these nanocomposites reported in literature. Mechanical results show that the incorporation of SWCNTs into a 3YTZP matrix produces an increase in the strain rate at high temperature with respect to monolithic zirconia. The creep resistance of these nanocomposites decreases with the improvement of the SWCNTs dispersion, where a smaller SWCNTs agglomerate size and consequently a higher concentration of carbon nanotubes surrounding the 3YTZP grain boundaries is found. This fact indicates that SWCNTs act as a lubricant making grain boundary sliding easier during deformation of these composites.

Keywords: Nanotubes; Zirconia; Processing; Mechanical properties; Creep.

*Corresponding author: miguelcr@icmse.csic.es. Instituto de Ciencia de Materiales de Sevilla, CSIC-Universidad de Sevilla, Avda. Américo Vespucio 49, 41092 Sevilla (Spain). Tel: Int-34-95 455 09 64, Fax: Int-34-95 461 20 97.

**Fellow of the ACS.

1. Introduction

The excellent physical properties (high strength, hardness, thermal-chemical stability and wear resistance) of ceramic materials make them suitable for multiple applications. Monolithic 3YTZP has been extensively studied since last decades, and grain boundary sliding GBS is recognized as being the primary deformation mechanism responsible for the high temperature superplastic behaviour accommodated by cationic diffusion throughout the lattice.[1,2] However, ceramics brittleness at low temperatures prevents from their use in many structural applications.[3] Hence, in the last decades there has been a steadily increasing interest to overcome this drawback by means of the incorporation of reinforcing elements as fibers, whiskers, carbon nanotubes (CNTs)... .[4-7] CNTs possess extraordinary mechanical, electrical and thermal properties[8-10] which have encouraged the researchers to process ceramic/CNTs composites with the aim of transferring these properties to the final material.

However, it is not clear if the incorporation of carbon nanotubes, either single-walled or multi-walled (MWCNTs), in a ceramic matrix produces a strengthening and toughening effect or not.[11-17] The underlying reason for this controversy arises from the reliability of the method used to measure the toughness of these ceramic/CNTs composites. Basically, techniques used to measure the fracture toughness are Vickers indentation fracture (VIF) and single edge notched beam (SENB) tests. Although VIF method has been widely used, it is assumed that SENB tests lead to a more reliable and lower fracture toughness values. In fact, some authors claimed that using alone Vickers indentation tests is not very suitable to quantify toughness in these composites because of their anomalous elastic/plastic response under indentation.[11,12,14] For instance, in Al_2O_3/SWNTs composites Vickers indentation gives higher fracture toughness values than those measured in fully dense pure Al_2O_3.[13] However, no increase is found from SENB tests.[14]

Together with this discrepancy on the fracture toughness method, it seems that there is a different toughening effect depending on the CNTs type, either single-walled or multi-walled, added to the 3YTZP ceramic matrix. On the one hand, Mazaheri *et al.*[17] by means of both VIF and SENB tests found a significant improvement of mechanical properties in 3YTZP/MWCNTs composites with respect to monolithic 3YTZP. They reported a 30% increment in the value of the Young's modulus and that the indentation fracture toughness improved by a factor of about 2. Such an effect was argued to be owed to the pinning effect of MWCNTs found by means of Vickers restricting grain boundary sliding. Sun *et al.*[15] found by means of Vickers indentation tests that hardness of these composites

decreased with increasing the weight content from 0.1 to 1 wt.% of MWCNTs and that there was no improvement in fracture toughness compared to monolithic 3YTZP. This apparent contradiction can be attributed to the scatter in the fracture toughness measurements owed to a different MWCNTs dispersion and to a low MWCNTs concentration. In fact, Mazaheri *et al.*[17] found that for MWCNTs concentrations lower than 1.5 wt.% mechanical behaviour of composites was similar to monolithic 3YTZP. On the other hand, the addition of SWCNTs in a 3YTZP ceramic matrix seems to produce the opposite effect, since Poyato *et al.*[16] recently reported a decrease in hardness and fracture toughness when increasing the SWCNTs content up to 10 vol% in 3YTZP/SWCNTs composites. They argued this result as a consequence of a SWCNT weakening effect on interfacial cohesion between ceramic grains.

Regarding the high temperature mechanical properties of ceramic/CNTs composites, most studies reported in literature are related to mechanical spectroscopy measurements. Thus, a decrease in the high temperature background in 3YTZP/MWCNTs composites and an increase in the shear modulus with respect to monolithic 3YTZP have been reported by different authors.[18-20] Daracktchiev *et al*.[18] performed mechanical loss measurements in monolithic 3YTZP, SiO_2 doped 3YTZP and 3YTZP with 5 wt.% of MWCNTs, obtaining for the latter a significant decrease in the internal friction due to [19] studied low frequency mechanical loss in fine-grained CNTs inclusions. Schaller *et al*. 3YTZP unreinforced and reinforced with 0.5 and 1.5 wt.% of MWCNTs or silicon carbide whiskers, observing a decrease in the mechanical loss level at 1600 K with respect to pure 3YTZP. A higher MWCNTs concentration (5 wt.%) was used by Taheri *et al*. [20] and they also obtained a remarkable lower damping level in this composite compared to monolithic 3YTZP. All these authors[18-20] attributed this decrease in the high temperature background to the pinning effect of MWCNTs on the grain boundary sliding. Consequently, they also associated these results to a higher creep resistance at high temperatures, in spite of the large difference between creep and mechanical spectroscopy experiments due to the much lower stresses involved in the latter. However, creep studies on 3YTZP/CNTs composites reported in literature are very scarce. Mazaheri *et al.*[21] performed creep tests at 1600 K and 6 MPa on monolithic zirconia (3YTZP) and zirconia containing different MWCNT quantities, ranging within 0.5 – 5 wt.%, and they reported a creep rate decrease of three orders of magnitude for the composite with the highest MWCNTs concentration compared to monolithic zirconia.

Nevertheless, much more investigations on Al_2O_3/CNT composites are reported in literature. A systematic study on the relationship between the presence of carbon in Al_2O_3 ceramic nanotubes and creep behaviour was performed by Zapata *et al.*[22] matrix containing SWCNTs. They reported that the strain rate exhibited by a 10 vol.% SWNT-reinforced Al_2O_3 composite was two orders of magnitude lower than pure alumina of the same grain size. That was attributed to the blocking of GBS and diffusion inhibition due to the presence of SWCNTs at the Al_2O_3 grain boundaries. On the contrary, Huang *et al.*[23] reported that un-deformable alumina ceramic showed promising superplastic behaviour even at temperatures as low as 1300 ºC by the addition of 0.5 wt% of BN nanotubes. This is evidence that the nature of nanotubes plays a crucial role in the final mechanical properties of the alumina composite. At this regard, Zhou *et al.*[24] studied the effect on the high temperature mechanical properties in Al_2O_3/MWCNTs composites depending on the different surface MWCNT-functionalization. They performed forging experiments at a constant stress of 65 MPa and heating up from 800 to 1400 ºC at 300 ºC/min in alumina composites containing either non-covalent or covalent functionalized-MWCNTs. It is worth emphasizing that this sort of experiments differs from creep tests since in the former samples cannot reach a stable microstructure, especially when the testing temperatures are higher than the sintering temperature, making difficult to evaluate and discern between the role of CNTs and microstructural changes on the mechanical properties. They reported that the creep behaviour of alumina can be mediated by CNTs through different surface functionalization, where non-covalent functionalization-dispersed carbon nanotubes make the alumina ceramics more ductile, whereas covalent functionalization of MWCNTs (acid-treated MWCNTs) enhance the creep resistance ability of the alumina matrix. However, these results seem not to be in agreement to what found Estili *et al*.[25] since they observed a much lower flow stress in 20 vol.% surface acid treated Al_2O_3/MWCNT composites than in pure alumina. But their result is not conclusive because, on the one hand tests were performed at higher temperatures than the sintering temperature and microstructural evolution of specimens takes place during deformation. On the other hand, in their constant cross head speed tests, grain boundary slip could not be fully accommodated by diffusion, leading to stress rising and generating cavitations.

So, nowadays there is a lack of reliable results on high temperature mechanical properties of ceramic/CNTs composites and a big debate about if the addition of CNTs leads to a reinforcement or not. Besides that, it is worth emphasizing that mechanical properties of nanocomposites are CNTs distribution dependent.[26] Thus, the powder processing routine and the sintering technique selected to

fabricate ceramic/CNTs composites should generate a homogeneous CNTs dispersion throughout of ceramic matrix, avoiding the formation of CNTs agglomerates and preserving the CNTs integrity.

The powder processing routine is a crucial step in the fabrication of ceramic/CNTs composites, since CNTs tend to agglomerate into parallel ropes or bundles due to van der Waals forces. So the major challenge of the processing routine is twofold, disentangle CNT bundles and from each other and distribute them uniformly throughout the ceramic matrix. Several processing routines are used: (i) conventional powder processing involving the use of ultrasound or ball milling, which could damage CNTs; (ii) sol-gel processing, involving the production of a sol containing ceramic particles, wherein CNTs are mixed and entrapped in the gel network; (iii) colloidal processing where CNTs and ceramic particles are in suspension and agglomerations are avoided by adjusting surface chemistry using dispersants, surfactants or an acid treatment. The later seems to lead to a better CNTs distribution.[27] In particular, Poyato *et al.*[16,28] used aqueous colloidal processing of SWCNTs and Al_2O_3 at a pH of 12, involving electrostatic repulsion between individual acid treated SWCNTs and individual Al_2O_3 ceramic particles due to their negative surface charge, obtaining a good CNTs dispersion throughout the ceramic matrix.

Related to sintering techniques, spark plasma sintering (SPS) is the most popular and mostly used to fabricate ceramic/CNTs composites because it allows fully dense composites at lower temperatures and shorter holding times, with high heating and cooling rates, and then ensuring CNT integrity after sintering.

The present study shows different powder processing methods to obtain 3YTZP containing 2.5 vol.% of SWCNTs sintered by Spark Plasma Sintering. The aim of this work is twofold: (i) obtaining an optimal CNT dispersion throughout the 3YTZP ceramic matrix. Aqueous colloidal processing and ball milling have been used to prepare the composites powders. Microstructure of the as-fabricated samples has been characterized by HRSEM, giving special emphasis to the SWCNTs distribution, in order to find which processing routine provides the best SWCNT, (ii) Mechanical characterization of samples to correlate the microstructure of 3YTZP/SWCNTs nanocomposites obtained following different powders processing, CNTs dispersion and creep resistance. Specimens have been crept at 1200 ºC and stresses between 9 and 40 MPa in a controlled argon atmosphere. It is worth emphasizing that there are not creep experimental results on 3YTZP/SWCNTs nanocomposites reported in

literature. Finally, the high temperature mechanical behaviour of these nanocomposites and monolithic zirconia are compared and discussed in this work.

2. Experimental Procedure

2.1. Starting materials

Commercially available 3 mol% yttria stabilized zirconia 3YTZP powder (Nanostructured and Amorphous Materials Inc., Houston, TX), with 40 nm average particle size and 99% purity, was annealed in air at 1250 ºC for one hour to remove the sintering additives from the starting powder and subsequently ball milled for 3 hours with a frequency of 25 vibrations/s (Model MM200, Retsch GmbH, Haan, Germany) to remove possible starting powder agglomerates generated during the previous annealing.

Two types of SWCNTs were used in this work. On the one hand, commercially available 90% purified SWNTs, with a typical bundle length of 0.5-1.5 μm and diameter between 4-5 nm, were provided by Carbon Solutions Inc. (Riverside, CA). The COOH-functionalization process we carried out was as follows: SWNTs were suspended for 24 hours at room temperature in a mixture of concentrated sulphuric acid (98 vol.%) and nitric acid (70 vol.%) in a 3:1 ratio. The suspension was sonicated for 8 hours in an ultrasonic bath and SWCNTs were collected on pore filter membranes (~20 nm) and washed in high-purity ethanol several times. Finally, they were dried either on hot plate at 70-80 ºC and homogenized in agate mortar (hereafter they are called SWCNTs-1a), or by means of freeze-drying technique (henceforth they are labelled SWCNTs-1b). On the other hand, commercial COOH functionalized SWCNTs (purity >95 vol.%), with ~1.5 nm in diameter and between 1 and 5 μm in length, provided by Nanolab Inc (Waltham, MA) which hereafter are labelled SWCNTs-2.

2.2. Powder processing methods

Basically, two processing methods were performed. On the one hand aqueous colloidal processing ACP,[28] where SWCNTs and 3YTZP powder were sonicated separately in two high pH solutions (distilled water + NH_3 solution until a pH=12) for 1 hour either in an ultrasonic bath or by means of

an ultrasonic probe (Model KT-600, Kontes Inc., Vineland, New Jersey). Later, they were suspended in the same high pH solution, and sonicated again for 30 min. Finally, the blend was dried either on hot plate stirring or by freeze drying. In the latter case, it is worth emphasizing that after mixing 3YTZP powder and SWCNTs in the high pH solution, a crucial step was to freeze immediately the solution to avoid the 3YTZP powder decantation. Immersing the solution into liquid nitrogen ensures that the freezing is fast enough to prevent this problem. On the other hand, ball milling has been also used to mix 3YTZP powder and CNTs, with a frequency of 25 vibrations/s, but for short enough times to preserve CNTs integrity.

Thus, different specimens have been processed depending on the SWCNTs type, the processing and the drying technique applied to the blend. The label and the processing routine followed for each specimen are detailed below and summarized in Table I.

- **1aHP**: SWCNTs-1a and 3YTZP powder were processed by ACP and sonicated using an ultrasonic bath. The blend was dried on a hot plate stirring at 70-80 ºC. Afterwards, composite powders were homogenized in agate mortar. 3YTZP/SWCNTs composites were processed following this routine in Ref. 16.

- **1bFD**: SWNTs-1b and 3YTZP powder were processed by ACP and sonicated in an ultrasonic bath. However, after sonication the solution was immediately frozen by immersion in liquid nitrogen and freeze-dried. Finally, the blend was homogenized by ball milling for 5 min with a frequency of 25 vibrations/s.

- **1bFD-probe** and **2FD-probe**: SWNTs-1b and 3YTZP powder or SWNTs-2 and 3YTZP powder were processed respectively following the same previous processing routine but using an ultrasonic probe instead of an ultrasonic bath.

- **1bM**: SWNTs-1b and 3YTZP powder were mixed by ball milling for 5 hours.

- **2M**: SWNTs-2 and 3YTZP powder were ball milled for 3.5 hours.

2.3. Sintering

Composite powders were sintered by Spark Plasma Sintering (Model Dr Sinter 1050, Sumitomo Coal Mining Co. LTD, Tokyo, Japan). They were loaded into a graphite die (10 mm inner diameter) and

a sheet of graphite paper was placed between the powders and die/punches to ease the specimen removal. The standard sintering parameters used were as follows: heating rate of 300 ºC min^{-1}; sintering temperature of 1250 ºC; holding time of 5 min; cooling rate of 50 ºC min^{-1} and 75 MPa of constant applied pressure under vacuum (10^{-2} mbar). For the sake of comparison, monolithic 3YTZP was sintered using the same conditions. The sintering temperature required to get full dense samples depends on the CNTs concentration, and in 3YTZP/CNTs literature it varies between 1250 and 1350 ºC.[15,17] In this work we have selected a sintering temperature of 1250 ºC for both monolithic 3YTZP and 3YTZP/SWCNTs nanocomposites (2.5 vol% of SWCNTs), and this has been enough to obtain rather dense specimens (relative density > 97%). Densities of the sintered specimens were measured by Archimedes' method taking a SWCNT density of 1.3 g/cm^3, as it was given by the providers.

2.4. Microstructural characterization

The microstructure of the samples was examined by light microscopy (Model Leica DMRE, Leica Microsystems GmbH, Germany), by conventional scanning electron microscopy SEM (Model JEOL 6460LV, JEOL USA Inc., MA, USA) and by high resolution scanning electron microscopy HRSEM (Model HITACHI S5200, Hitachi High-Technologies Corporation, Tokyo, Japan). Cross-section specimens were prepared for microstructural observations. Surfaces were first ground and then polished with diamond paste down to 1 μm. Those polished surfaces devoted to characterizing the zirconia grains were thermally etched at 1150 ºC for 20 minutes in air to reveal grain boundaries. Fracture cross-section specimens were also investigated by HRSEM, and by Raman spectroscopy to study SWCNTs integrity after sintering, using a dispersive microscope (Model LabRAm Horiba Jobin Yvon, Horiba Ltd, Kyoto, Japan). Measurements were done with a green laser (He–Ne 532.14 nm), 20-mW, 600 g/mm grating and without filter. A 100× objective and a confocal pinhole of 100 μm were used. The Raman spectrometer was calibrated using a silicon wafer.

The microstructural study comprises a double characterization in the case of composites: (i) the analysis of 3YTZP grain morphology and (ii) the study of SWNTs integrity and their dispersion throughout the 3YTZP matrix, together with the analysis of the morphology and density of CNTs agglomerates. The grain morphology characterization was made by measuring the equivalent planar diameter ($d=(4\times area/\pi)^{1/2}$), and the shape factor ($F=4\pi\times area/(perimeter)^2$) from HRSEM micrographs on no less than 300 grains. These same parameters were evaluated to characterize CNTs

agglomerates along with their surface density, estimated from the area fraction covered by them in low magnification SEM micrographs and also by means of light microscope observations.

2.5. Mechanical tests

The mechanical behaviour of the processed materials was investigated by uniaxial compression creep tests on samples cut and ground as parallelepipeds of approximate dimensions 5 × 2.5 × 2.5 mm^3. The creep tests were performed on a prototype creep machine[29] at 1200 ºC, stresses ranging between 9 and 40 MPa and in a controlled argon atmosphere to avoid the combustion of SWCNTs and the oxidation of the 3YTZP ceramic matrix. The working atmosphere was prepared at room temperature, using several vacuum cycles (10^{-6} Pa) followed by the introduction of argon. These cycles were repeated at 500 °C to eliminate any products of possible degassing of the elements inside the working chamber. Once reached the testing temperature (1200 ºC) and after thermal stabilisation of the system, stress changes were made, and a steady state characterized by a constant strain rate $\dot{\varepsilon}$ was obtained for each experimental condition.

The creep curves were analysed using the standard phenomenological creep equation:

$$\dot{\varepsilon} = A\frac{\sigma^n}{d^p}\exp\left(-\frac{Q}{KT}\right) \quad (1)$$

where *A* is a stress and temperature independent term reflecting the dependence of the strain rate on the microstructural features of the material (composition, amount and physical properties of glassy phases, grain morphology, etc.), σ the applied stress, *d* the mean grain size, *k* the Boltzmann's constant, and T the absolute temperature. The parameters n, p, and Q (generically known as creep parameters) are, respectively, the stress and grain size exponents, and the apparent activation energy for creep. These parameters together with the microstructural changes after deformation are the fingerprints of possible deformation mechanisms. In this work only the stress exponent *n* has been determined since here we are focussed on measuring the creep resistance of these composites; however, a more detailed study about their creep behaviour is underway.[30]

3. Results and Discussion

3.1. Microstructural characterization and CNTs dispersion

CNTs agglomerates are observed in all the specimens; however, their characteristics (surface density, size, shape factor) strongly depend on the powder processing routine. An example is shown in Fig. 1 where light microscope observations of specimens 1bM and 1bFD-probe clearly indicate that in the latter SWCNTs are much better dispersed since SWCNTs agglomerates exhibit a much lower surface density and a considerably smaller size. A study of CNTs agglomerates for each specimen fabricated in this work is shown in Table II. As it is observed, 1bM and 2M specimens show the highest surface densities, 4.6 ± 1.5 and 4.3 ± 2.0 % respectively, with almost the biggest SWCNTs agglomerate size. Moreover, by HRSEM these nanocomposites do not show a good CNTs distribution because they are mainly forming agglomerates (Fig. 2h) and they are scarcely observed on 3YTZP grain boundaries (Fig. 2c and 2f). This is evidence that ball milling seems not to be very suitable to mix 3YTZP powder and SWCNTs.

In the case of aqueous colloidal processing ACP, no significant improvement is obtained for 1aHP and 1bFD composites with respect to the ball milled 1bM and 2M specimens, since by HRSEM only a slight increase of CNTs is observed surrounding 3YTZP grain boundaries (Fig. 2.b and 2.d), and the surface density and size of CNTs agglomerates still exhibit high values (Table II). However, the optimal CNTs distribution has been clearly achieved when a combination of ultrasonic probe and freeze-drying technique are applied to the blend processed by ACP, i.e. in 1bFD-probe and 2FD-probe specimens. These specimens exhibit a surface density of SWCNTs agglomerates more than one order of magnitude lower than other specimens. Moreover, the average agglomerate size for these specimens is significantly smaller. Thus, HRSEM observations on 1bFD-probe and 2FD-probe specimens indicate that they possess an optimal CNTs dispersion (Fig. 2e and 2g) since CNTs are observed homogeneously distributed throughout the 3YTZP ceramic matrix. With regard to the shape factor of SWCNTs agglomerates; all the nanocomposites exhibit a value close to 0.7, except 1bM specimen whose shape factor value is slightly lower. That could be the result of being ball milled for 5 hours during the processing routine which probably led to barely more elongated SWCNT agglomerates prior to sintering.

The different degrees of SWCNTs dispersion should influence the final microstructure of the nanocomposites, since SWCNTs surrounding 3YTZP grains can inhibit the ceramic grain growth during sintering.[31,32] Fig. 2 shows the microstructure of the sintered samples, where 3YTZP grains are faceted with sharp triple points. In case of nanocomposites, CNTs are forming bundles surrounding 3YTZP grains. However, their dispersion throughout the matrix strongly depends on the

processing routine followed to their fabrication, being optimal for 1bFD- probe and 2FD-probe specimens (Fig. 2e and 2g).

Table II summarizes the microstructural study performed on the sintered materials. A microstructure composed by equiaxed grains with submicrometric grain size smaller than 0.3 microns is observed in all the samples (Fig. 2). Monolithic 3YTZP has an average grain size of about 0.27 microns. However, this value is slightly lower for 3YTZP/SWCNTs nanocomposites mixed by ball milling (1bM and 2M), which probably generated a decrease in the particle size of the starting 3YTZP powder. Also, a smaller average grain size is observed in specimens where 3YTZP powder and SWCNTs were mixed by ACP using an ultrasonic probe and subsequent freeze-dried (1bFD-probe and 2FD-probe). As observed in Table II, these specimens exhibit the best CNTs dispersion, so they can impede more efficiently the 3YTZP grain growth during sintering.[31,32] On the contrary, 1aHP was not ball milled and the processing routine did not provide a good SWCNTs dispersion in the grain boundaries, so it makes sense that the same grain size is observed than for monolithic 3YTZP, both fabricated under the same sintering conditions. The shape factor is also quite similar for all the sintered materials. So, the presence of 2.5 vol.% SWCNTs in a 3YTZP ceramic matrix slightly modifies the grain size of the sintered materials when SWCNTs are homogenously distributed throughout of the matrix.

It is worth emphasizing that the lowest relative density values are obtained for 3YTZP/SWCNTs nanocomposites exhibiting the highest surface density of SWCNTs agglomerates, as shown in Table II. SWCNTs agglomerates impede 3YTZP powder to go inside and fill the empty space between CNTs and consequently producing a decrease in the density of these materials. It is remarkable that porosity has not been observed in an isolated way but always associated to the presence of SWCNTs agglomerates (Fig. 2h). That means that the surface density values of SWCNTs agglomerates measured from micrographs are overestimated, since they also contain the contribution coming from the cavities and the empty space between CNTs. So, removing this contribution it is possible to estimate the SWCNTs vol.% forming agglomerates, and consequently the SWCNTs vol.% that are effectively well distributed surrounding YTZP grain boundaries. For instance, ball milled 1bM and 2M specimens exhibit a surface density of SWCNTs agglomerates of about ~ 4.5%. The relative density of these nanocomposites is ~ 97.5%, so there is ~ 2.5% of cavities and empty space inside these materials associated to the presence of SWCNT agglomerates, which should be removed from the surface density measured in these nanocomposites. Then, about ~ 2 vol.% of SWCNTs are

forming agglomerates. Since nanocomposites contain 2.5 vol.% of SWCNTs, that means that only the 0.5 vol.% of them are surrounding 3YTZP grain boundaries, indicating that ball milling is not very suitable to obtain a good SWCNTs distribution. On the contrary, for 1bFD-probe and 2FD-probe specimens almost all the SWCNTs are well distributed throughout the 3YTZP ceramic matrix since less than 0.2 vol.% of them are forming agglomerates. So ACP, using an ultrasonic probe and the freeze-drying technique, clearly is the most effective routine to disentangle bundles of nanotubes and minimize the formation of SWCNTs agglomerates, and consequently to provide an optimal SWCNTs distribution.

3.2. CNTs integrity

HRSEM observations suggest that SWCNTs have not undergone severe damage since SWCNTs filaments are observed in all the specimens sintered in this work, either distributed throughout the 3YTZP ceramic matrix or forming agglomerates depending on the processing routine. Furthermore, Fig. 3a and 3b show the Raman spectra measured in the composites sintered with CNTs provided by Carbon Solutions Inc. and by Nanolab Inc., respectively. Raman spectra measured in monolithic 3YTZP ceramic and in SWCNTs are included for comparison. Peaks at 165, 260, 320, 465, 610 and 643 cm^{-1} corresponding to the six Raman bands predicted for theoretical tetragonal zirconia are observed in the Raman spectra of nanocomposites. They also show the typical mode bands owed to the presence of CNTs: radial breathing, and the G mode (~1550-1600 cm^{-1}) which mode bands located about 150-200 cm^{-1} corresponds to the tangential shear mode of carbon atoms. Graphite has only one single symmetric G mode at 1580 cm^{-1}; while for SWCNTs, G bands have a low-energy branch and then an unsymmetrical G mode which implicates the existence of SWCNTs. The D mode in the Raman spectrum (~1350 cm^{-1}) of graphite can also be observed. This mode is due to longitudinal optical phonons from the vicinity of the K-point in the Brillouin zone, and defects are needed for this elastic scatter. So the higher intensity ratio I_D/I_G and the more symmetrical G mode, then the more severe damage in the SWCNTs structure. Comparing the spectra measured in the nanocomposites and in the SWCNTs (provided by Carbon Solutions Inc. or by Nanolab Inc.) we can conclude that the I_D/I_G ratio does not increase significantly, indicating that SWCNTs keep their integrity after the processing and sintering process.

At this regard it is worth emphasizing that SWCNTs provided by Nanolab Inc. exhibit the D mode band which it is not perceptible in SWCNTs provided by Carbon Solutions Inc. This could be

attributed to a better CNTs quality provided by the latter company. What is clear is that ball milling seems not to be very useful to generate a good CNTs dispersion and its use is very risky since it could produce damages in SWCNTs. The effect of ball milling on the structure and morphology of SWCNTs was studied by Pierard *et al*.[33] They reported that SWCNTs do not resist very long milling times. Just after 2-3 hours under a frequency of 50 vibrations/s they observed a progressive destruction of their tubular structure, and consequently a severe decrease in their average length, to form multi-layered polyaromatic carbon. In this work, ball milling has been carried out for 3.5 hours in 2M specimen and for 5 hours in 1bM sample, both at 25 vibrations/s what is close but below the limit reported by Pierard *et al.* [33] to preserve the SWCNTs integrity. We have not achieved a good CNTs dispersion by means of this technique, especially in 2M specimen, whose Raman spectra fluctuated drastically depending on the point on which the Raman measurements were acquired. We obtained either signal coming from SWCNTs agglomerates (grey line) or coming from 3YTZP grains (black line) (Fig. 3b), what it is indicative that SWCNTs are not well distributed. Fig. 3b also contains a Raman spectrum of the 2FD-probe specimen after the creep test. As it is observed, it exhibits the characteristic mode bands due to the presence of SWCNTs, indicating that during the creep test CNTs keep their integrity and they do not undergo damages. Fig. 4 is a HRSEM micrograph of the 2FD-probe specimen after the creep test, where we can clearly see SWCNTs bundles surrounding 3YTZP grain boundaries in Fig. 4b and Fig. 4c.

3.3. CNTs dispersion and creep resistance

The powder processing methods followed to obtain 3YTZP/SWCNTs nanocomposites have led to microstructures with different degrees of SWCNTs dispersion, and consequently they should have a different mechanical behaviour since mechanical are SWNTs distribution dependent. [21,26] Fig 5a shows the properties of nanocomposites creep curves at 1200 ºC for 2FD-probe nanocomposite and monolithic 3YTZP specimens. The steady-state strain rate is clearly reached by the specimens after each stress change, which allows to obtain the stress exponents *n*. Fig. 5b shows log–log plot of the steady-state creep rate versus stress for monolithic 3YTZP and the 3YTZP/SWCNTs nanocomposites fabricated following the processing routines described in section 2.2. For each specimen, in this plot the linear regression slope of the strain rate-stress data provides the stress exponent *n* shown in Fig. 5b (see equation (1)). Nanocomposites containing SWCNTs-1b or SWCNTs-2 processed following the same routine show no difference in their mechanical behaviour. It is remarkable that monolithic

3YTZP exhibits a higher creep resistance than any 3YTZP/SWCNTs nanocomposite fabricated in this work.

Regarding Fig. 5b and taking into account the results shown in Table II, it is clear that the best CNTs dispersion the lower creep resistance. Thus, 2M and 1bM nanocomposites, where the 3YTZP powder and CNTs were mixed by ball milling which led to the worst CNTs dispersion, exhibit the higher creep resistance among all the nanocomposites. 1aHP and 1bFD nanocomposites, with a better CNTs dispersion compared to 1bM and 2M specimens, experience a higher strain rate under the same stress, i.e., a lower creep resistance. Finally, nanocomposites processed by ACP using the ultrasonic probe and the freeze-drying technique (1bFD-probe and 2FD-probe), with an optimal CNTs dispersion and homogeneous distribution throughout the ceramic matrix, exhibit the lowest creep resistance. For instance, at stresses of about 20 MPa, the strain rate of these nanocomposites is about 60 times higher than that corresponding to the monolithic 3YTZP.

The stress exponent *n* has been calculated for all the deformed samples. Monolithic 3YTZP shows a stress exponent n equal to 2.3, in agreement with results previously reported,[1,2] where deformation was achieved primarily by grain boundary sliding GBS accommodated by cationic diffusion throughout the lattice. The stress exponent *n* obtained for 3YTZP/SWCNTs nanocomposites is ranged between 1.9 and 2.7, which is close to what has been obtained for monolithic 3YTZP. These *n* values evidence that GBS is operating in both, monolithic 3YTZP and 3YTZP/SWCNT nanocomposites, at the temperature and stress range of our experiments. The deformation and accommodation mechanisms on these nanocomposites are investigated in a more complete study which will be reported elsewhere.[30]

In section 3.1, it is shown that ball milling or a good SWCNTs dispersion throughout the 3YTZP matrix result in a moderate decrease in the grain size of the final sintered material. This decrease should have effects on the mechanical behaviour of 3YTZP/SWCNTs nanocomposites compared to monolithic 3YTZP, since it is well known that a refinement in the grain size generally produces a strain rate enhancement. Under the same experimental conditions (T and σ) and using equation (1), an estimation of this enhancement α can be writing as follows:

$$\alpha = \frac{\dot{\varepsilon}_c}{\dot{\varepsilon}_m} \approx \left(\frac{d_m}{d_c}\right)^p \qquad (2)$$

where ($\dot{\varepsilon}_c$, d_c) and ($\dot{\varepsilon}_m$, d_m) are the strain rate and de average grain size of the nanocomposite and the monolithic 3YTZP, respectively. The grain size exponent *p* values reported in the literature for this material vary between 1 and 3.[2] Then, considering the average grain size values shown in Table II, roughly an enhancement α between 1 and 3 is obtained in the strain rate of nanocomposites compared to monolithic 3YTZP.

From experimental data shown in Fig. 5b, the enhancement in the strain rate of nanocomposites, due to a smaller grain size with regards to monolithic 3YTZP, could only explain the mechanical behaviour of 1bM and 2M specimens (Fig. 5b). However, for the other nanocomposites the effect of a smaller grain size clearly cannot explain by itself the increase in the strain rate experimentally observed. In particular, this is the case for 1bFD-probe and 2FD-probe specimens, where the strain rate is about 60 times higher compared to monolithic 3YTZP. EDX measurements performed on 3YTZP/SWCNTs composites revealed that no impurities had been introduced during the processing and sintering, at least in a perceivable concentration.

Then, the lower creep resistance exhibited by nanocomposites compared to monolithic 3YTZP may attest the weak interfacial bonding between SWCNTs and 3YTZP ceramic grain boundaries and the detachment of SWCNTs within bundles surrounding 3YTZP grains. So taking into account that the accommodation mechanism takes place by diffusion throughout the lattice,[1,2] then the presence of SWCNTs at 3YTZP grain boundaries has no influence on the accommodation mechanism and only is related to the grain boundary sliding, acting as a lubricant. Also, glide between CNTs located at the grain boundaries could facilitate GBS. Specimens mixed by ball milling show a mechanical behaviour closer to monolithic 3YTZP. This is because SWCNTs dispersion is not homogenous and carbon nanotubes are entangled forming agglomerates and leaving most of 3YTZP grains with no CNTs. So these specimens deform like the monolithic 3YTZP, although the CNTs agglomerates make grain boundary sliding easier at their surrounding and then a lower creep resistance is observed. Moreover, these specimens mixed by ball milling show a slight decrease in the grain size with regards to monolithic zirconia that could also explain their lower creep resistance. Nevertheless, specimens with the highest SWCNTs dispersion, 1bFD-probe and 2FD-probe, show a much lower creep resistance. In these specimens CNTs are much better distributed on the 3YTZP ceramic matrix, surrounding most of the 3YTZP grains, and then facilitating the grain boundary sliding.

These results are not in agreement with the published one by Mazaheri *et al*.,[21] since they reported an enhancement in the creep resistance of 3YTZP by the addition of MWCNTs. Nevertheless, on the one hand specimens were crept at 1327 ºC, which was higher than the sintering temperature (1250 ºC for composites containing a MWCNTs concentration below 3 wt.%) and consequently an evolution of their microstructures during the tests is expected. The microstructural evolution depends on the MWCNT concentration. In their results, composites with the highest MWCNT concentration quickly reached the steady-state strain rate but that was not the case for monolithic zirconia and the composite with 0.5 wt.% of MWCNTs, which seem to be both in the transitory state. In their work, the microstructural characterization of the deformed specimens is not shown making difficult to interpret the effect of MWCNTs on the operating deformation mechanisms during the creep tests. On the other hand, in our work SWCNTs have been used instead of MWCNTs. The addition of either SWCNTs or MWCNTs to a 3YTZP ceramic matrix may influence differently its high temperature mechanical behaviour. There is experimental evidence of this different effect in the room temperature mechanical behaviour of 3YTZP/CNT composites. Thus, the presence of SWCNTs in a 3YTZP ceramic matrix leads to a decrease in the hardness and toughness due to a weak interfacial bonding between SWCNTs and 3YTZP grains[16], whereas the addition of MWCNTs in a 3YTZP ceramic matrix has a strengthening and toughening because they hinder the grain boundary sliding.[17] That could also explain the disagreement between our results and the predictions of a higher creep resistant for 3YTZP/MWCNT nanocomposites compared to monolithic 3YTZP by means of mechanical spectroscopy measurements performed by different authors.[18-20]

However, no work on 3YTZP/SWCNTs composites and their creep behaviour has been so far reported. The only work concerning a ceramic containing SWCNTs was but using a Al_2O_3 matrix. In their work, creep resistance performed by Zapata *et al.*, [22] for Al_2O_3/SWCNTs composites was found to be two orders of magnitude higher than for pure Al_2O_3 of the same grain size. Taking into account that in both 3YTZP and Al_2O_3 the deformation mechanism is GBS, it seems that there is a controversy in the results since the addition of SWCNTs in 3YTZP produces a softening and in Al_2O_3 a strengthening. Nevertheless, in Al_2O_3 GBS is accommodated by diffusion where the preferred path is grain boundaries, and the presence of SWCNTs produces a shift in the dominant accommodation mechanism from diffusional creep to power law creep (PLC), involving the activation of dislocation motion. This leads to a strengthening of the matrix.[22] In 3YTZP, the accommodation mechanism takes place by diffusion throughout the lattice,[1,2] and the only effect of the presence of SWCNT is

related to the grain boundary sliding, acting as a lubricant and producing the softening observed in our experiments.

4. Conclusions

Several powder processing methods have been followed to optimize the CNTs dispersion into a 3YTZP ceramic matrix. Ball milling seems not to be an useful technique to mix 3YTZP powder and SWCNTs since it cannot provide a good CNTs dispersion throughout the 3YTZP ceramic matrix. However, an optimal CNTs distribution on the ceramic matrix has been obtained by aqueous colloidal processing using an ultrasonic probe and the freeze-drying technique. The weak interfacial bonding between SWCNTs and 3YTZP together with the easy glide within SWCNTs bundles located at the grain boundaries make 3YTZP/SWCNTs nanocomposites less creep resistant.

Acknowledgements

This work was financially supported by the Spanish "Ministerio de Economía y Competitividad" through the projects MAT2009-11078, MAT2012-34217 and the project from the Andalucia Government P12-FQM-1079. M. C-R thanks the JAE-doc contract awarded by the Spanish CSIC.

References

1. A. Domínguez-Rodríguez, D. Gómez-García and F. Wakai "High Temperature Plasticity in Yttria Stabilised Tetragonal Zirconia Polycrystals (Y-TZP)," *Int. Mater.Rev.*, **58**, 399-417 (2013).

2. M. Jiménez-Melendo, A. Domínguez-Rodríguez and A. Bravo-León, "Superplastic Flow of Fine-Grained Yttria-Stabilized Zirconia Polycrystals: Constitutive Equation and Deformation Mechanisms," J. Am. Ceram. Soc., **81**, 2761–76 (1998).

3. B. R. Lawn, "Fracture of brittle solids", 2nd ed. Cambridge: Cambridge University Press (1990).

4. K. M. Prewo, "Fiber-Reinforced Ceramics: New Opportunities for Composite Materials," Am. Am. Ceram. Bull, **68**, 395-400 (1989).

5. J. J. Mason and R. O. Ritchie, “Fatigue Crack Growth Resistance in SiC Particulate and Whisker Reinforced P:M 2124 Aluminum Matrix Composites,” Mater. Sci. Eng. A, **231**, 170–182 (1997).

6. A. Peigney, “Composite Materials: Tougher Ceramics with Nanotubes,” Nature Materials, **2**, 15-6 (2003).

7. J. Cho, A. R. Boccaccini and M. S. P. Shaffer, “Ceramic Matrix Composites Containing Carbon Nanotubes,” *J. Mater. Sci*., **44**, 1934-51 (2009).

8. M. M. J. Treacy, T. W. Ebbesen and J. M. Gibson, “Exceptionally High Young’s Modulus Observed for Individual Carbon Nanotubes,” *Nature,* **381**, 678-80 (1996).

9. A. Thess, R. Lee, P. Nikolaev, H. Dai, P. Petit and J. Robert, “Crystalline Ropes of Metallic Carbon Nanotubes,” *Science*, **273**, 483-87 (1996).

10. R. H. Baughman, A. A. Zakhidov and W. A. de Heer, “Carbon Nanotube-the Route Toward Applications,” *Science*, **297**, 787-92 (2000).

11. N. P. Padture and W. A. Curtin, “Comment on Effect of Sintering Temperature on a Single-Wall Carbon Nanotube-Toughened Alumina Based Composite,” *Scr. Mater*., **58**, 989-90 (2008).

12. N. P. Padture, “Multifunctional Composites of Ceramics and Single-Walled Carbon Nanotubes,” *Adv. Mater*., **21**, 1767-70 (2009).

13. G. D. Zhan, J. D. Kuntz, J. Wan and A. K. Mukherjee, “Single Wall Carbon Nanotubes as Attractive Toughening Agents in Alumina-Based Nanocomposites,” *Nature Mater.*, **2**, 38-42 (2003).

14. X. Wan, N. P. Padture and H. Tanaka, “Contact-Damage-Resistant Ceramic/Single-Wall Carbon Nanotubes and Ceramic/Graphite Composites,” *Nature Mater.*, **3**, 539-44 (2004).

15. J. Sun, L. Gao, M. Iwasa, T. Nakayama and K. Niihara, “Failure investigation of carbon nanotube/3YTZP nanocomposites,” *Ceram. Int*., **31**, 1131-34 (2005).

16. R. Poyato, A. Gallardo-López, F. Gutierrez-Mora, A. Morales-Rodríguez, A. Muñoz and A. Domínguez-Rodríguez, “Effect of High SWNT Content on the Room Temperature Mechanical Properties of Fully Dense 3YTZP/SWNT Composites,” *J. Eur. Ceram.*, **34**, 1571-79 (2014).

17. M. Mazaheri, D. Mari, R. Schaller, G. Bonnefont and G. Fantozzi, “Processing of Yttria Stabilized Zirconia Reinforced with Multi-Walled Carbon Nanotubes with Attractive Mechanical Properties,” *J. Eur. Ceram. Soc.*, **31**, 2691-98 (2011).

18. M. Daraktchiev, B. Van de Moortèle, R. Schaller, E. Couteau and F. Forró, “Effects of Carbon Nanotubes on Grain Boundary Sliding in Zirconia Polycrystals,” *Adv. Mater.*, **17**, 88-91 (2005).

19. R. Schaller and C. Ionascu, “High-Temperature Mechanical Loss and Creep Behaviour of Fine-Grained Zirconia-Containing Nano-Sized Reinforcements,” *Mater. Sci. Eng. A*, **521**, 217-20 (2009).

20. M. Taheri, M. Mazaheri, F. Golestani-Fard, H. Rezaie and R. Schaller, “High/Room Temperature Mechanical Properties of 3Y-TZP/CNTs Composites,” *Ceram. Int.*, **40**, 3347-52 (2014).

21. M. Mazaheri, D. Mari, R. Hesabi, R. Schaller and G. Fantozzi, “Multi-Walled Carbon Nanotube/Nanostructured Zirconia Composites: Outstanding Mechanical Properties in a Wide Range of Temperature,” *Comp. Sci. Tech.*, **71**, 939-45 (2011).

22. E. Zapata-Solvas, R. Poyato, D. Gómez-García, A. Domínguez-Rodríguez, V. Radmilovic and N. P. Padture, “Creep-Resistant Composites of Alumina and Single-Wall Carbon Nanotubes,” *Appl. Phys. Lett.*, **92**, 111912, 3pp (2008).

23. Q. Huang, Y. S. Bando, X. Xu, T. Nishimura, C. Y. Zhi, C. Tang, F. Xu, L. Gao and D. Golberg, “Enhancing Superplasticity of Engineering Ceramics by Introducing BN Nanotubes,” *Nanotechnology*, **18**, 485706, 7pp (2007).

24. X. Zhou, L. Li, L. Shen, J. Zhou, J. Zhang, A. K. Mukherjee, C. Xiang, H. Tang and Q. Huang, “Superplastic Behaviour of Alumina Composites Mediated by Carbon Nanotubes,”. *Nano-Micro Lett.*, **5**, 174-81 (2013).

25. M. Estili, Y. Sakka, W. W. Wu, T. Nishimura, H. Yoshida and A. Kawasaki, “Perfect High-Temperature Plasticity Realized in Multiwalled Carbon Nanotube Concentrated α-Al_2O_3 Hybrid,” *J. Am. Ceram. Soc.*, **96**, 1904-08 (2013).

26. E. Zapata-Solvas, D. Gómez-García, R. Poyato, Z. Lee, M. Castillo-Rodríguez, A. Domínguez-Rodríguez, V. Radmilovic and N. P. Padture, “Microstructural Effects on the Creep Deformation of Alumina/Single-Wall Carbon Nanotubes Composites,” *J. Am. Ceram. Soc.*, **93**, 2042-47 (2010).

27. E. Zapata-Solvas, D. Gómez-García and A. Domínguez-Rodríguez, "Towards Physical Properties Tailoring of Carbon Nanotubes-Reinforced Ceramic Matrix Composites," *J. Eur. Ceram. Soc*., **32**, 3001-20 (2012).

28. R. Poyato, A. L. Vasiliev, N. P. Padture, H. Tanaka and T. Nishimura, "Aqueous Colloidal Processing of Single-Wall Carbon Nanotubes and their Composites with Ceramics," *Nanotechnology*., **17**, 1770-77 (2006).

29. M. Castillo-Rodríguez, A. Muñoz and A. Domínguez-Rodríguez, "Correlation Between Microstructure and Creep Behaviour in Liquid-Phase-Sintered α-Silicon Carbide," *J. Am. Ceram. Soc*., **89**, 960-67 (2006).

30. M. Castillo-Rodríguez, A. Muñoz, A. Domínguez-Rodríguez, "High Temperature Mechanical Behaviour of 3YTZP/SWCNT Nanocomposites," in progress.

31. A. Datye, K. H. Wu, G. Gomes, V. Monroy, H. T. Lin, J. Vleugels and K. Vanmeensel, "Synthesis, Microstructure and Mechanical Properties of Yttria Stabilized Zirconia (3YTZP) – Multi-Walled Nanotube (MWNTs) Nanocomposite by Direct insitu Growth of MWNTs on Zirconia Particles," *Comp. Sci. Tech*., **70**, 2086-92 (2010).

32. A. Duszová, J. Dusza, K. Tomasek, G. Blugan and J. Kuebler, "Microstructure and Properties of Carbon Nanotube/Zirconia Composite," *J. Eur. Ceram. Soc*., **28**, 1023-27 (2008).

33. N. Pierard, A. Fonseca, J. F. Colomer, C. Bossuot, J. M. Benoit, G. van Tendeloo, J. P. Pierard and J. B. Nagy, "Ball Milling Effect on the Structure of Single Walled Carbon Nanotubes," *Carbon*, **42**, 1691–97 (2004).

FIGURE CAPTIONS

Fig. 1. Light microscope micrographs of a) 1bM and b) 1bFD-probe specimens, where it is clearly observed that the former exhibits a much higher surface density and a bigger size of SWCNTs agglomerates.

Fig. 2. HRSEM micrographs of a) monolithic 3YTZP and the 3YTZP/SWCNTs nanocomposites: b) 1aHP, c) 1bM, d) 1bFD, e) 1bFD-probe, f) 2M and g) 2FD-probe (see section 2.2). h) CNTs agglomerate in 1bM specimen. They are observed in samples where CNTs are not well distributed.

Fig. 3. Raman spectra of 3YTZP/SWCNTs nanocomposites fabricated using CNTs provided by a) Carbon Solution Inc., and by b) Nanolab Inc. This latter also contains the Raman spectrum of a sample after mechanical testing which clearly indicates that no CNTs damages are generated during the creep test.

Fig. 4. a) HRSEM micrograph of the 2FD-probe sample after mechanical testing. Micrographs taken at higher magnification in b) and c) show CNTs bundles located on the 3YTZP grain boundaries, attesting that CNTs keep their integrity after the creep test.

Fig. 5. a) Creep curves at 1200ºC for 2FD-probe nanocomposite and monolithic 3YTZP. b) Strain rate versus stress logarithmic plot for monolithic 3YTZP and the 3YTZP/SWCNTs nanocomposites. Stress exponent n is indicated for each nanocomposite.

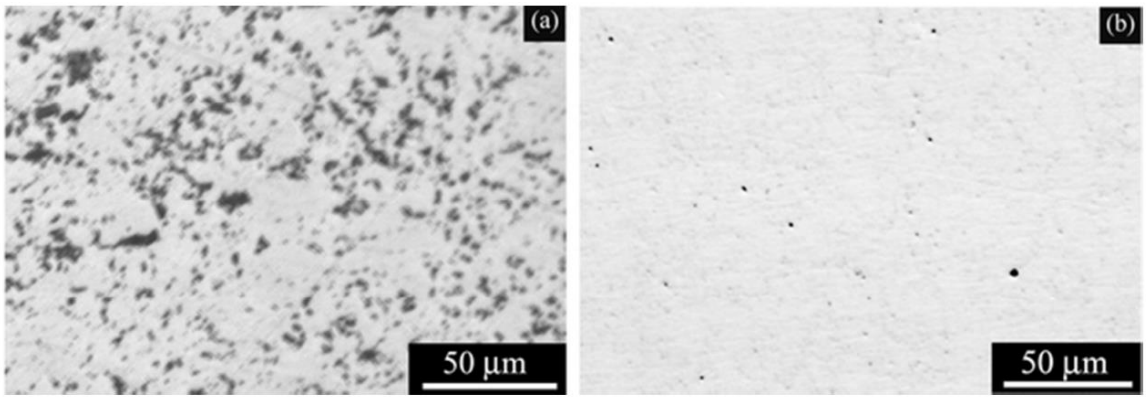

Fig. 1. Light microscope micrographs of a) 1bM and b) 1bFD-probe specimens, where it is clearly observed that the former exhibits a much higher surface density and a bigger size of SWCNTs agglomerates. 55x18mm (300 x 300 DPI)

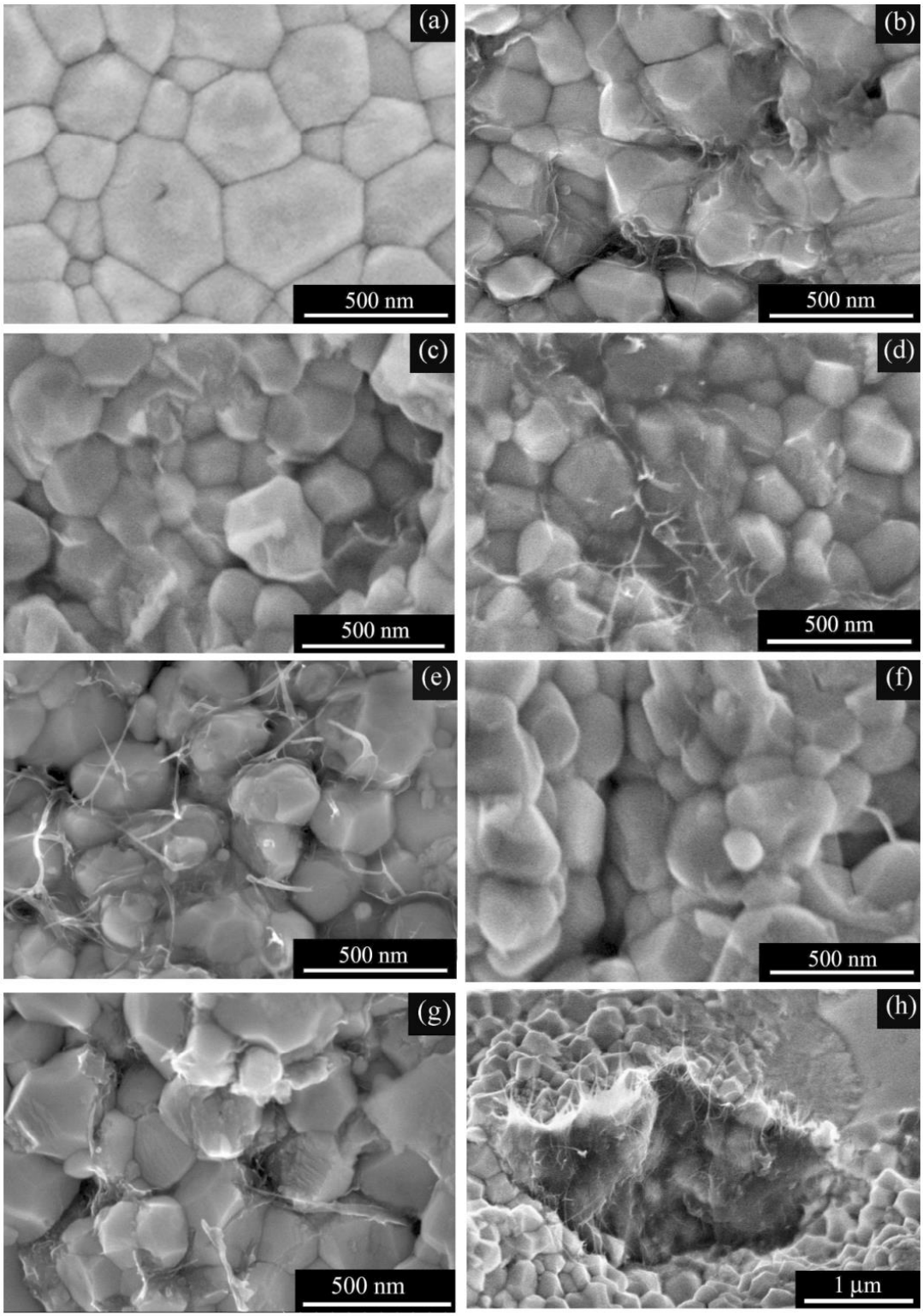

Fig. 2. HRSEM micrographs of a) monolithic 3YTZP and the 3YTZP/SWCNTs nanocomposites: b) 1aHP, c) 1bM, d)1bFD, e) 1bFD-probe, f) 2M and g) 2FD-probe (see section 2.2). h) CNTs agglomerate in 1bM specimen. They are observed in samples where CNTs are not well distributed. 172x245mm (300 x 300 DPI)

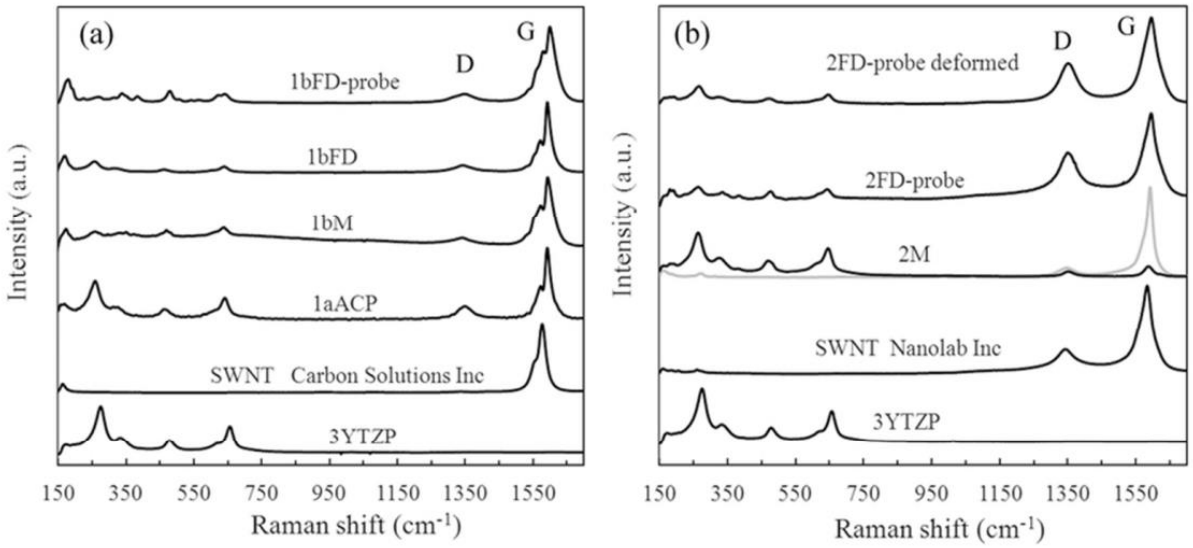

Fig. 3. Raman spectra of 3YTZP/SWCNTs nanocomposites fabricated using CNTs provided by a) Carbon Solution Inc., and by b) Nanolab Inc. This latter also contains the Raman spectrum of a sample after mechanical testing which clearly indicates that no CNTs damages are generated during the creep test. 74x34mm (300 x 300 DPI)

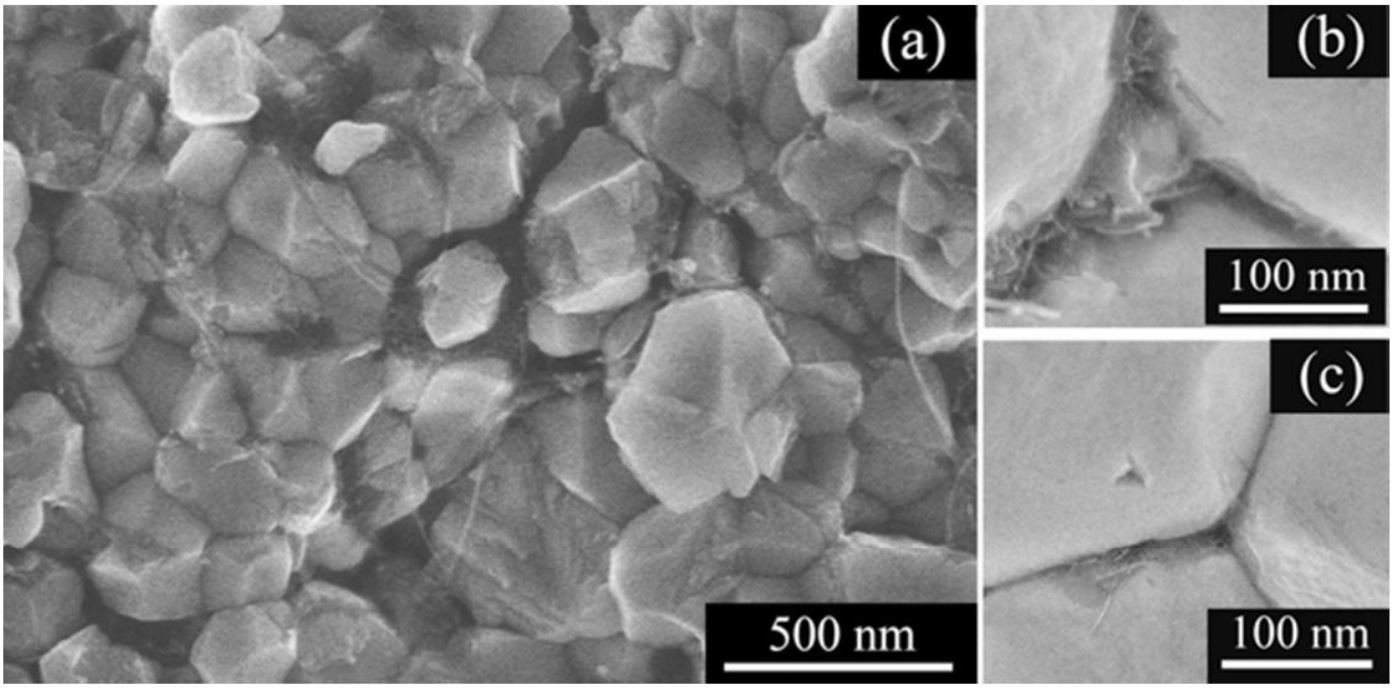

Fig. 4. a) HRSEM micrograph of the 2FD-probe sample after mechanical testing. Micrographs taken at higher magnification in b) and c) show CNTs bundles located on the 3YTZP grain boundaries, attesting that CNTs keep their integrity after the creep test. 56x27mm (300 x 300 DPI)

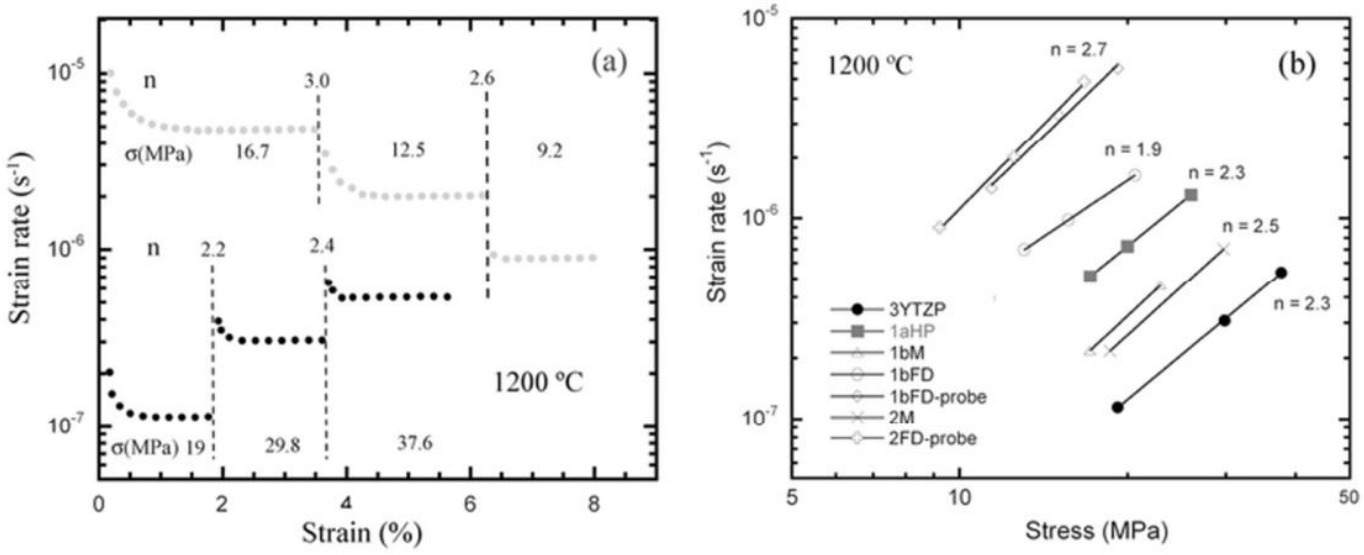

Fig. 5. a) Creep curves at 1200ºC for 2FD-probe nanocomposite and monolithic 3YTZP. b) Strain rate versus stress logarithmic plot for monolithic 3YTZP and the 3YTZP/SWCNTs nanocomposites. Stress exponent n is indicated for each nanocomposite. 67x27mm (300 x 300 DPI)

Table I. It is shown schematically the SWCNTs type, the powder mixing process (aqueous colloidal processing ACP or ball milling) and how the blend was dried for each composite.

Composite	SWNTs			Mixing process			Drying process	
				ACP				
	1a	1b	2	Ultrasonic bath	Ultrasonic probe	Ball milling	Hot plate stirring	Freeze drying
1aHP	X			X			X	
1bM		X				X		X
1bFD		X		X				X
1bFD-probe		X			X			X
2M			X			X		X
2FD-probe			X		X			X

Table II. Relative density ρ_r, morphological parameters (grain or agglomerate size *d* and shape factor *F*) and surface density of SWCNTs agglomerates ρ_s obtained for the as-sintered materials.

Material	**ρ_r ± 0.5 (%)**	**3YTZP grains**		**SWCNTs agglomerates**		
		d (μm)	**F**	**ρ_s (%)**	**d (μm)**	**F**
3YTZP	99.5	0.27 ± 0.10	0.72 ± 0.07			
1aHP	97.3	0.27 ± 0.11	0.72 ± 0.07	3.3 ± 0.5	3.8 ± 0.5	0.71 ± 0.17
1bM	97.8	0.22 ± 0.08	0.72 ± 0.07	4.6 ± 1.5	2.5 ± 0.1	0.51 ± 0.18
1bFD	99.3	0.24 ± 0.09	0.72 ± 0.08	2.1 ± 0.4	2.4 ± 0.4	0.64 ± 0.19
1bFD-probe	99.5	0.22 ± 0.09	0.74 ± 0.07	0.2 ± 0.1	0.5 ± 0.1	0.72 ± 0.15
2M	97.1	0.19 ± 0.07	0.73 ± 0.09	4.3 ± 2.0	2.5 ± 0.2	0.72 ± 0.16
2FD-probe	99.5	0.20 ± 0.08	0.72 ± 0.07	0.2 ± 0.1	0.5 ± 0.2	0.73 ± 0.14